HHS Public Access

Author manuscript

Cancer Res. Author manuscript; available in PMC 2018 August 01.

Published in final edited form as:

Cancer Res. 2017 August 01; 77(15): 4014–4025. doi:10.1158/0008-5472.CAN-16-2885.

IGFBP7 Deletion Promotes Hepatocellular Carcinoma

Maaged Akiel[1], **Chunqing Guo**[1], **Xia Li**[1], **Devaraja Rajasekaran**[1], **Rachel G. Mendoza**[1], **Chadia L. Robertson**[1], **Nidhi Jariwala**[1], **Fang Yuan**[1], **Mark A. Subler**[1], **Jolene Windle**[1], **Dawn K. Garcia**[2], **Zhao Lai**[2], **Hung-I Harry Chen**[2], **Yidong Chen**[2,3], **Shah Giashuddin**[4], **Paul B. Fisher**[1,5,6], **Xiang-Yang Wang**[1,5,6], and **Devanand Sarkar**[1,5,6,7]

[1]Department of Human and Molecular Genetics, Virginia Commonwealth University, Richmond, VA 23298, USA

[2]Greehey Children's Cancer Research Institute, University of Texas Health Science Center San Antonio, San Antonio, TX 78229

[3]Department of Epidemiology and Biostatistics, University of Texas Health Science Center San Antonio, San Antonio, TX 78229

[4]Department of Pathology, New York Presbyterian Health System at Weill Cornell Medical College, New York, NY

[5]Department of VCU Massey Cancer Center, Virginia Commonwealth University, Richmond, VA 23298, USA

[6]Department of VCU Institute of Molecular Medicine (VIMM), Virginia Commonwealth University, Richmond, VA 23298, USA

Abstract

Activation of IGF signaling is a major oncogenic event in diverse cancers, including hepatocellular carcinoma (HCC). In this setting, the insulin-like growth factor binding protein IGFBP7 inhibits IGF signaling by binding the IGF-1 receptor (IGF-1R), functioning as a candidate tumor suppressor. IGFBP7 abrogates tumors by inhibiting angiogenesis and inducing cancer-specific senescence and apoptosis. Here we report that Igfbp7-deficient mice exhibit constitutively active IGF signaling, presenting with pro-inflammatory and immunosuppressive microenvironments and spontaneous liver and lung tumors occurring with increased incidence in carcinogen-treated subjects. Igfbp7 deletion increased proliferation and decreased senescence of hepatocytes and mouse embryonic fibroblasts, effects that were blocked by treatment with IGF-1 receptor inhibitor. Significant inhibition of genes regulating immune surveillance was observed in Igfbp7−/− murine livers, which was associated with a marked inhibition in antigen cross-presentation by Igfbp7−/− dendritic cells. Conversely, IGFBP7 overexpression inhibited growth of HCC cells in syngeneic immunocompetent mice. Depletion of CD4+ or CD8+ T lymphocytes abolished this growth inhibition, identifying it as an immune-mediated response. Our findings define an immune component of the pleiotropic mechanisms through which IGFBP7 suppresses HCC. Furthermore,

[7]**Corresponding author:** Devanand Sarkar, 1220 East Broad St, Box 980035, Richmond, VA 23298, Tel: 804-827-2339, Fax: 804-628-1176, devanand.sarkar@vcuhealth.org.

Disclosure: All authors have no potential conflicts.

they offer a genetically based preclinical proof of concept for IGFBP7 as a therapeutic target for immune management of HCC.

Keywords

IGF signaling; antigen presentation; tumor suppression; inflammation; mouse model

Introduction

Evasion from immune surveillance is an important mechanism facilitating tumor development and progression (1). Three equally important events are necessary for immune evasion, the masking of neo-antigens, downregulation of antigen presentation machinery, and irresponsiveness to Interferon-γ (IFN-γ)-mediated killing by immune cells (2). Tumor antigenic peptides are generally produced in the cytosol via processing by proteasomes that contain interferon-γ-inducible subunits LMP-2, LMP-7 and LMP-10 (3). The 8–9 amino acids antigen peptides thus produced are translocated by transporters associated with antigen processing (TAP-1 and TAP-2) to the endoplasmic reticulum (ER) where the peptides are assembled with MHC class I heavy chain and β_2-microglobulin light chain and are transported to the cell surface to be presented to $CD8^+$ cytotoxic T lymphocytes (CTL). The components of the antigen presentation pathway, such as TAP1/2 and LMP2/7, are downregulated in cancers, including HCC, resulting in a loss of immune-surveillance and initiation and progression of the disease (4).

Insulin-like growth factor (IGF) signaling plays an important oncogenic role in hepatocellular carcinoma (HCC) (5). Insulin-like growth factor binding protein-7 (IGFBP7) is a secreted protein that binds to IGF-1 receptor (IGF-1R) and blocks activation by IGFs (6). IGFBP7 functions as a tumor suppressor in a variety of cancers, including HCC, where its expression is markedly downregulated (7–9). Genomic deletion and promoter hypermethylation cause downregulation of IGFBP7 in HCC (7,10). Recombinant IGFBP7 (rIGFBP7) protein induces senescence and/or apoptosis and inhibits angiogenesis in diverse cancers either *in vitro* or in nude mice xenograft models (8,9,11). Stable overexpression of IGFBP7 in aggressive human HCC cells led to inhibition in IGF signaling, induced senescence, inhibited proliferation and resulted in profound inhibition in xenograft growth in nude mice which was accompanied by marked inhibition in angiogenesis (7). Intratumoral injection of an adenovirus expressing IGFBP7 (Ad.IGFBP7) eradicated both injected tumors as well as non-injected tumors established in the other flank of nude mice indicating that IGFBP7 not only has direct effect on primary cancer but also exerts a ‘by-stander’ anti-tumor effect (12). However, the mechanism by which IGFBP7 exerts this ‘by-stander’ effect remains to be determined.

In this manuscript we describe the generation and characterization of an Igfbp7 knockout (Igfbp7−/−) mouse which establishes the tumor suppressor functions of IGFBP7 and unravels a novel role of IGFBP7 in regulating an anti-tumor immune response. These studies indicate that IGFBP7 inhibits cancer by pleiotropic mechanisms and might be an effective therapeutic for HCC and other cancers.

Materials and methods

Generation of Igfbp7−/− mouse

Igfbp-7−/− mouse was created in a pure C57BL/6 background using a Cre-loxP strategy (Fig. S1). All animal studies were approved by the Institutional Animal Care and Use Committee at Virginia Commonwealth University, and were performed in accordance with the Animal Welfare Act, the PHS Policy on Humane Care and Use of Laboratory Animals, and the U.S. Government Principles for the Utilization and Care of Vertebrate Animals Used in Testing, Research, and Training.

Primary cells isolation and culture conditions

All primary cells were used immediately after isolation and were mycoplasma free. Primary mouse hepatocytes were isolated and cultured in Williams E Medium containing $NaHCO_3$, L-glutamine, insulin (1.5 mmol/L), and dexamethasone (0.1 mmol/L) as described (13). Kupffer cells were isolated from liver homogenates by centrifuging at 500 RPM for 10 min (14). The supernatant containing immune cells was sorted for $CD11b^+F4/80^+$ cells using FACSAria II (BD Biosciences). Mouse embryonic fibroblasts (MEFs) were isolated as described from (E13.5 embryos) and were cultured in Dulbecco's Modified Eagle's Medium (DMEM) containing 10% fetal bovine serum (FBS) (15). Bone marrow-derived macrophages and peritoneal macrophages were isolated according to standard protocols (16). Bone marrow cells were isolated from femurs of C57BL/6 mice and were differentiated into macrophages using RMPI-1640 medium supplemented with 10% heat-inactivated FBS and 20% L929 conditioned media for 7days. At day 7, the media was changed to complete RPMI-1640 containing 10% heat-inactivated FBS. Macrophages were cultured in complete media for at least 12 hours prior to using for experiments. Stellate cells were isolated according to standard protocol (17). All primary cells were isolated from male mice of 6–12 wks of age, were cultured at 37C° and in 5% CO_2 with 100% humidity and were used for experiments at 60–80% confluence. Cells from DEN-treated animals were obtained at 20–32 wks of age.

N-nitrosodiethylamine (DEN) induced HCC

A single dose of 10μg/g body weight of DEN was administered intraperitoneally (i.p.) to 14 days old male pups. The animals were monitored and euthanized at 32 wks of age. Serum liver enzymes were analyzed in the Molecular Diagnostic Laboratory, Department of Pathology, VCU using standard procedures.

RNA extraction, cDNA synthesis and Quantitative Real-time PCR

Total RNA was extracted using the QIAGEN RNeasy Mini Kit (QIAGEN; Cat# 74104). 2μg of RNA was used for cDNA synthesis using ABI cDNA Synthesis Kit (Applied Biosystems). Q-RT-PCR was performed using an ABI ViiA7 fast real-time PCR system, and Taqman gene expression assays using predesigned best coverage Taqman probes for standard gene expression (Applied Biosystems) according to the manufacturer's protocol. All mRNA levels were normalized by GAPDH mRNA levels.

RNA Sequencing (RNA-seq)

RNA, extracted from livers of 3 adult mice per group, was used. RNA-Seq library was prepared using Illumina TruSeq RNA Sample Preparation Kit and sequenced on Illumina HiSeq2000 platform. RNA-Seq libraries were pooled together to aim about 25 to 40 million read passed filtered reads per sample. All sequencing reads were aligned with their reference genome (UCSC mouse genome build mm9) using TopHat2. Bam files from alignment were processed using HTSeq-count to obtain the counts per gene in all samples. The counts for all samples were read into R software using DESeq package. For each condition a pairwise test was performed using the functions in DESeq and plot distributions were analyzed using Reads Per Kilobase Million (RPKM) values. Data were filtered on the basis of low count or low RPKM value (<40 percentile). Genes showing log2 fold-change of >1.5 or <−1.5, FDR of <0.1 and p-value of <0.05 were selected. A complete list of differentially regulated genes is available in GSE85427 (https://www.ncbi.nlm.nih.gov/geo/query/acc.cgi?token=ctoloyiiznwbtgt&acc=GSE85427)

In vitro antigen cross presentation of bone marrow-derived dendritic cells (BMDCs) and T-cell priming

BMDCs were isolated as described (18). Bone marrow-derived cells were differentiated into dendritic cells by culturing in RPMI-1640 medium containing granulocyte macrophage colony-stimulating factor (GM-CSF; 20ng/ml) for 8 days. Day 8 Igfbp7+/+ and Igfbp7−/− BMDCs were loaded with 1μg/mL gp100 (25–33a.a.) peptide for 3 h, followed by 500 ng/mL lipopolysaccharide (LPS) for 2 h (priming). LPS was washed before co-culturing the BMDCs with pmel-17 T lymphocytes at a molar ratio of 1:10, 1:20 and 1:40 (DC:TC) for 60 hours. In a second experiment, gp100-loaded BMDCs were treated or not with rIGFBP7 protein (R&D) for 3 h followed by OSI-906 (4 μmol/L) for 2 h and LPS (500 ng/mL) for 2 h. The cells were washed and co-cultured with pmel-17 T cells for 60 h. Supernatants were collected at 48 h for ELISA. Cells were pulsed with 0.5 μCi/well [^{3}H]-thymidine for the last 16 h of incubation. Proliferation was measured by [^{3}H]-thymidine incorporation in triplicate wells.

Establishment of stable Igfbp7 overexpressing clone in Hepa1-6 cells

Hepa-1-6 cell line (CRL-1830) was obtained from ATCC and was cultured as instructed. Mouse Igfbp7 (NM_001159518) expression plasmid was obtained from Origene Technologies, Inc. (MR222256). Hepa1-6 cells were transfected with 8μg of mIgfbp7 expression plasmid DNA and corresponding empty vector using FuGENE® HD transfection reagent at a ratio of 3.5:1 (reagent:DNA). Transfected cells were selected in 450μg/ml G418 for 4 weeks to establish BP7-OE pooled clone.

Xenograft studies in syngeneic mice

C57L/J mice were purchased from The Jackson Laboratory. Control and BP7-OE pooled clones of Hepa1-6 cells (4×10^6) were injected subcutaneously into the right dorsal flank of C57L/J mice. Five mice per group were used. Tumor volume was measured by the following formula: $\pi/6 \times (\text{small diameter})^2 \times (\text{large diameter})$. Mice were monitored twice a week and

euthanized after 4 weeks at which point the tumors were harvested. Immune cells infiltration was determined by FACS as described (19).

$CD8^+$ and $CD4^+$ depletion assays

S.c. xenografts were established using BP7-OE clones in C57L mice. Depletion of $CD8^+$ and $CD4^+$ cells was performed by injecting 200 μg of neutralizing antibodies i.p. on days 1, 5, 12 and 19 as described (19). Tumors were collected 4 weeks after tumor implantation. Neutralizing antibodies were obtained from Bioxcell, $CD8^+$ Ab (Clone: 2.43 Catalog #BP0061), $CD4^+$ Ab (Clone: GK1.5 Catalog #BP0003-1).

Immunohistochemistry (IHC) and immunofluorescence (IF) assays

IHC was performed on formalin-fixed paraffin-embedded (FFPE) sections as described (20) using the following antibodies: AFP (Santa cruz: sc-15375), PCNA (Cell signaling #13110), c-Myc (Cell signaling #13987), CD31 (Dako #JC70A), F4/80 (AbD Serotec #MCA497RT), glutamine synthetase (Sigma #G2781) and IGFBP7 (R&D systems #MAB21201). IF was performed on cells cultured in 4-chamber slides for hepatocytes (collagen-1 coated) and MEFs using antibodies against p65 (Cell signaling #8242) and γ-H2AX (Cell signaling #5438). The images were taken by a confocal laser scanning microscope. Antibody dilutions were used as recommended by the manufacturer.

Senescence-associated β-galactosidase (SA-β-Gal) assay

Hepatocytes were cultured for 8 days and SA-β-Gal activity was measured as described (7).

Cell proliferation, BrdU incorporation and colony formation assays

Cells (1×10^3) were plated in each well of a 96 well plate for measuring proliferation by a standard MTT assay (7). BrdU incorporation was measured using BrdU Cell Proliferation Assay Kit (Cell signaling #6813) according to the manufacturer's protocol. Colony formation assay was performed by plating 1×10^4 MEFs on 6 cm dishes and culturing for 4 weeks.

Western blotting analysis

Cell lysates and tissue extracts were prepared and Western blotting was performed as described (20). The primary antibodies used were: p-AKT (Cell signaling #4060), AKT (Cell signaling #4685), pERK (Cell signaling #9101), ERK (Cell signaling #4695). p-IGF-1Rβ (Cell signaling #6113), IGF-1Rβ (Cell signaling #9750), GAPDH (Santa Cruz #sc-166545), EF1α (Millipore #05-235), p-GSK3β (Cell Signaling #5558), GSK3β (Cell Signaling #12456), p65 NF-κB (Cell signaling #5438), p-p65 (Cell signaling #8242), Cyclin D1 (Cell Signaling #2978), Cyclin E1 (Cell signaling #4129), Arginase-1 (Santa cruz #sc-18355), Myc-tag (Cell signaling #2276), p-STAT1 (Cell signaling #9167), STAT1 (Cell signaling #14994), Igfbp7 (R&D systems #MAB21201) and β-actin (Sigma Aldrich #A5316). Antibodies were diluted as recommended by the manufacturer. Densitometric analysis was performed by ImageJ software.

In vitro treatment of cells

Recombinant mouse IGF-1 (R&D systems #Q8CAR0) was used at 20ng/ml for signaling experiments and 100ng/ml for cell proliferation experiments. LPS (sigma Aldrich #L3024) was used at 200ng/ml. OSI-906 (Selleckchem #S1091) was used at 4 μmol/L. In vitro DEN was used at 10ng/mL.

Cell cycle analysis

MEFs (1×10^5) were synchronized in serum-free media for 18 h and released into complete growth media. Cells were washed with PBS and fixed in 70% ethanol for 30 min at −20°C. The fixed cells were washed three times with PBS and were incubated with PBS containing 10 μg/mL RNase A for 30 min at 37C° following which cells were incubated with 30 μg/mL propidium iodide (PI) for 30 min in the dark. The samples were acquired in a FACSCanto II system. For each measurement 10,000 cells were acquired and the data were analyzed using the FACSDiva software.

Fluorescence-activated cell sorting (FACS) analysis

To analyze immune cell population livers from 5 months old DEN-injected littermates were perfused and resuspended into a single cell suspension as described (13). The cell suspension was subjected to FACS analysis as described (19). The s.c. xenograft tumor tissues were digested with collagenase D (10 mg/mL) and DNase I (100 mg/mL), and cell suspensions were filtered through a 70 mm cell strainer prior to FACS analysis (19). Antibodies were obtained from Biolegend: CD4 (GK1.5), CD8 (2.43), INF-γ (XMG1.2), Ly6G (1A8), Ly6C (HK1.4), CD80 (16-10A1), CD86 (GL-1), CD11b (M1/70), CD11c (N418), F4/80 (BM8), CD3 (17A2), NK1.1 (PK136), B220 (RA3-6B2) and Gr1 (RB6-8C5).

NF-κB luciferase reporter assay

NF-κB luciferase reporter assay was performed in Igfbp7+/+ and −/− hepatocytes exactly as described (20). Experiments were performed in triplicates with two independent experiments.

Co-injection of HCC cells and bone marrow-derived macrophages in NOD *scid* Gamma (NSG) mice

Dihxy cells ($1X10^6$), developed from DEN-injected C57BL/6 mice in Dr. Karin's laboratory (21), were co-injected with bone marrow derived macrophages ($10 X 10^4$ or $5 X 10^4$) from Igfbp7+/+ and Igfbp7−/− mice subcutaneously in 7 wks old male NSG mice and tumor development were monitored for 7 weeks. Tumor volume was measured with calipers using the formula: $(Width)^2 \times length/2$. For each group 5 mice were used.

Statistical Analysis

Data were presented as the mean ± SD and analyzed for statistical significance using two-tailed student t-test. For canonical pathway analysis the p-value was calculated using the right-tailed Fisher Exact Test.

Results

Generation of Igfbp7−/− mouse

We generated Igfbp7−/− mice on C57BL/6 background by targeting promoter region and exon 1 of mIgfbp7 gene by Cre-loxP strategy (Fig. S1A–B, 1A–C). IHC staining of the Igfbp7+/+ liver showed more IGFBP7 staining in interstitial cells when compared to hepatocytes (Fig. 1C). Q-RT-PCR analysis demonstrated significantly more Igfbp7 mRNA expression in stellate cells and macrophages compared to hepatocytes (Fig. 1D). In liver and spleen, macrophage marker F4/80 positive cells showed positive staining for IGFBP7 further indicating that non-parenchymal cells are the major source of IGFBP7 (Fig. S1C). The levels of other IGFBPs and IGF-1 and IGF-2 mRNAs were similar in Igfbp7+/+ and Igfbp7−/− mice (Fig. S1D).

Loss of Igfbp7 increases spontaneous tumorigenesis without affecting normal development

Igfbp7−/− mice were viable and fertile having normal litter size. Histological analysis of internal organs from 8 weeks old mice did not show any discernable difference between Igfbp7+/+ and Igfbp7−/− mice indicating that Igfbp7 may not play a role in normal development (Fig. S2A). However, when monitored for 24 months, Igfbp7−/− mice (3 out of 10) developed spontaneous tumors in liver and lung while no tumors were detected in Igfbp7+/+ mice (n = 7) (Fig. 1E). The tumors in the liver showed complete loss of hepatic architecture indicating HCC (Fig. 1E). At this age, splenic architecture was distorted in Igfbp7−/− mice compared to +/+. Additionally, increased infiltration of immune cells in the tissue microenvironment of liver, lung and kidney was observed in Igfbp7−/− mice suggesting increased inflammation (Fig. 1E). In 24 months old liver and lung, increase in Il6 mRNA levels (marker of inflammation) was detected in both liver and lung tumors, but increase in α-feto protein (Afp) mRNA levels (marker of HCC) was observed only in liver tumors in Igfbp7−/− mice indicating that the lung tumors are primary tumors and not metastatic lesions from the liver (Fig. 1F). Increased staining for glutamine synthetase (a marker for HCC) and increased infiltration of macrophages (determined by F4/80 staining) was observed in 24 months old Igfbp7−/− liver sections compared to Igfbp7+/+ liver sections (Fig. S2B–C). Staining of lung tumors for F4/80 identified macrophages in between large tumor cells and the tumors showed strong positive staining for the proliferation marker PCNA and increased expression of angiogenesis marker Vegf in Igfbp7−/− but not in Igfbp7+/+ (Fig. S2D–F).

Loss of Igfbp7 increases proliferation and prevents senescence

We next checked the effect of genetic deletion of Igfbp7 on cell proliferation and senescence. Igfbp7−/− mouse embryonic fibroblasts (MEFs) showed increased proliferation as measured by MTT and colony formation assays when compared to Igfbp7+/+ (Fig. 2A). Similarly, Igfbp7−/− hepatocytes showed increased proliferation by MTT assay and increased BrdU incorporation upon IGF-1 treatment *versus* Igfbp7+/+ (Fig. 2B). Mouse hepatocytes do not proliferate *in vitro* and starts undergoing senescence by 96 h. At day 8 of culture ~80% of Igfbp7+/+ hepatocytes showed senescence versus only ~30% Igfbp7−/− hepatocytes (Fig. 2C and S3A). As a corollary, γ-H2AX positive nuclei were significantly

reduced in Igfbp7−/− MEFs after 12 hours of serum starvation (Fig. 2D and S3B). To check the effect of Igfbp7 deletion on cell cycle progression, MEFs were synchronized in serum free media for 24 hours following which they were released in complete growth media and subjected to cell cycle analysis. At 18 and 36 h post-release there was a significant decrease in cells in G_1 phase and a corresponding increase in cells in G_2/M phase in Igfbp7−/− MEFs compared to Igfbp7+/+ MEFs indicating that Igfbp7−/− MEFs cycle faster than their wild type counterparts (Fig. 2E).

Loss of Igfbp7 activates the IGF-1 signaling pathway

Igfbp7+/+ and Igfbp7−/− hepatocytes were treated with recombinant mouse IGF-1 (20ng/ml). Constitutive activation of IGF-1R and downstream Akt and GSK3β was observed in Igfbp7−/− hepatocytes, and there was a further increase in IGF-1R, Akt and GSK3β activation in Igfbp7−/− hepatocytes, compared to Igfbp7+/+, at 5 min of exposure to IGF-1 suggesting that Igfbp7 null hepatocytes have increased propensity for activation of the IGF-1 pathway (Fig. 2F). In both cell types activation persisted until 60 min. Analysis of livers of adult mice also showed increased activation of Akt and its downstream target GSK3β further confirming constitutive activation of IGF-1 signaling in Igfbp7−/− mice (Fig. 2G and Fig. S4A). Constitutive activation of Akt, GSK3β and ERK was also observed in Igfbp7−/− hepatocytes, macrophages and MEFs compared to Igfbp7+/+ (Fig. 2H and Fig. S4B). Since Igfbp7−/− MEFs cycle faster than Igfbp7+/+ MEFs, we checked the levels of cyclin D1 (CCND1) and cyclin E1 (CCNE1), which facilitate G_1 to S cell cycle progression. Increased levels of CCND1 and CCNE1 was observed in Igfbp7−/− MEFs *versus* Igfbp7+/+ thus explaining the accelerated cell cycle progression in the former (Fig. 2H and Fig. S4B). We next checked how constitutive activation of IGF-1 signaling pathway modulates response of Igfbp7−/− MEFS to OSI-906, a dual kinase inhibitor of IGF-1R and insulin receptor (INSR). Igfbp7−/− MEFS were more sensitive to growth inhibition by OSI-906 compared to Igfbp7+/+ suggesting that Igfbp7−/− MEFs might have preferential addiction to IGF signaling (Fig. 2I). Overall, these results indicate that activation of the IGF-1 signaling pathway contributes to increased proliferation upon Igfbp7 deletion.

Loss of Igfbp7 results in markedly accelerated DEN-induced HCC

Since aged Igfbp7−/− mice develop spontaneous HCC, we further analyzed HCC development upon exposure to the hepatocarcinogen N-nitrosodiethylamine (DEN), a well-established HCC model (22,23). HCC was induced in Igfbp7+/+, +/− and −/− littermates by a single i.p. injection of DEN (10 μg/gm) when the mice were two weeks of age. At 32 weeks, Igfbp7−/− mice demonstrated a marked increase in both number and size of hepatic nodules when compared to the other genotypes (Fig. 3A–B). This increase in hepatic nodules contributed to increased liver to body weight ratio in Igfbp7−/− mice (Fig. 3C). Liver enzymes, aspartate aminotransferase (AST) and alanine aminotransferase (ALT), and serum total protein were significantly increased in Igfbp7−/− mice *vs* +/+ and +/− mice (Fig. 3D–E). Histological analysis of the liver showed extensive abnormality in liver architecture showing pleomorphic, hyperchromatic nuclei with increased infiltration of immune cells and abnormal blood vessel formation (Fig. 3F and Fig. S5A). Increased staining for AFP, proliferating cell nuclear antigen (PCNA; proliferation marker), c-MYC, CD31 (angiogenesis marker) and F4/80 (macrophage marker) was observed in Igfbp7−/− liver

sections when compared to Igfbp7+/+ indicating increased proliferation, angiogenesis, inflammation and development of frank HCC (Fig. 3F). Increased staining for glutamine synthetase was also observed in DEN-treated Igfbp7−/− livers compared to Igfbp7+/+ (Fig. S5B). To exclude the possibility that the increased HCC development in Igfbp7−/− mice is because of increased sensitivity to DEN we analyzed liver functions 48 hours after injection of DEN. Both Igfbp7+/+ and −/− littermates showed similar levels of changes in AST, ALT and Alkaline Phosphatase (ALP), a marker of acute liver damage, suggesting that littermates of both genotypes respond similarly to DEN-induced liver injury (Fig. S5C). DEN needs to be metabolically activated by CYP2E1 in zone 3 hepatocytes. Cyp2e1 mRNA levels were similar in Igfbp7+/+ and −/− livers (data not shown) suggesting that altered metabolism of DEN does not underlie differential tumorigenic response.

Igfbp7 deletion creates an inflammatory and immunosuppressive tumor microenvironment

DEN-induced HCC is an inflammatory-type of HCC in which damaged hepatocytes release cytokines, mainly IL-1β, which stimulate Kupffer cells to release IL-6 and TNFα by activating NF-κB signaling (24–26). In this context, we analyzed immune cell profile in Igfbp7+/+ and −/− mice by fluorescence-activated cell sorting (FACS). Examination of 8 weeks old naïve liver and spleen showed no significant difference in $CD8^+$ and $CD4^+$ T cells, natural killer (NK) cells, B cells, dendritic cells (DCs), splenic and liver macrophages, and myeloid-derived suppressor cells (MDSCs), indicating that IGFBP7 may not be required for immune cell development (Fig. S6A–B). However, upon examining the livers of DEN-treated mice at 20 weeks of age, a time-point before the development of overt hepatic nodules but having microscopic tumors as evidenced by increased AFP and c-Myc expression (Fig. S6C), we found a significant increase in Kupffer cells ($CD11b^{high}$/$F4/80^{low}$), infiltrating macrophages ($CD11b^{low}$/$F4/80^{high}$) and $CD11b^+$ monocytes ($Ly6G^-$/$Ly6C^+$) in Igfbp7−/− livers compared to +/+ livers (Fig. 4A). These results suggest that Igfbp7−/− mice have an inflammatory and immunosuppressive tumor microenvironment. M-MDSCs mediate immune suppressive function through L-arginine depletion by increasing expression of arginase-1 (ARG1) that abrogate antitumor responses by T cells (27). Indeed, DEN-treated Igfbp7−/− livers showed substantially increased levels of ARG1 compared to Igfbp7+/+ (Fig. S6D). This increased immune suppressive environment might contribute to a decrease in liver-infiltrating NK cells as well as $CD4^+$ and $CD8^+$ T cells (Fig. 4A).

The inflammatory environment in Igfbp7−/− cells were further checked at gene expression levels. Il6, Il1b, Tnfa and c-Myc (marker of proliferation) mRNAs showed significantly increased levels in the livers of DEN-treated Igfbp7−/− livers when compared to +/+ at 32 weeks (Fig. 4B). Igfbp7−/− hepatocytes, isolated at 24 wks after DEN treatment, and Igfbp7−/− Kupffer cells, isolated at 5 wks after DEN treatment, also showed increased levels of Il6, Il1b and Tnfa *versus* Igfbp7+/+ (Fig. 4B). Primary hepatocytes treated *in vitro* with DEN for 24 h showed significantly increased levels of Il1b and Tnfa, but not Il6, in Igfbp7−/− compared to Igfbp7+/+ indicating that Igfbp7−/− hepatocytes respond more to DEN-treatment in terms of generating cytokines leading to a robust activation of Kupffer cells generating Il6 (Fig. 4C, top). We treated macrophages with IL-1β (10 ng/ml) and measured Il6 and TNFa mRNA levels. Basal Il6 and TNFa levels were significantly higher in Igfbp7−/− macrophages versus +/+ (Fig. 4C, bottom). IL-1β treatment induced Il6 and TNFa mRNA

expression in both Igfbp7+/+ and −/− macrophages. However, the magnitude of induction was significantly more in Igfbp7−/− macrophages when compared to +/+. While inflammatory cytokine levels were similar in 6 weeks old Igfbp7+/+ and Igfbp7−/− livers, they were higher in 24 weeks old Igfbp7−/− livers compared to Igfbp7+/+ indicating that Igfbp7 deficiency with age creates a precancerous milieu for development of spontaneous HCC (Fig. S7A).

It is well-established that NF-κB is the pivotal regulator of inflammation-driven HCC and other cancers (26,28). Under basal condition, p50/p65 NF-κB resides in the cytoplasm and upon stimulation translocates to the nucleus. In Igfbp7+/+ hepatocytes, p65 NF-κB was located exclusively in the cytoplasm, while some nuclear staining of p65 was detected in Igfbp7−/− hepatocytes (Fig. 4D). Upon stimulation with lipopolysaccharide (LPS) p65 translocated to the nucleus in both cells. However, the magnitude of translocation was more robust in Igfbp7−/− hepatocytes compared to Igfbp7+/+. To quantify these changes we measured NF-κB luciferase reporter activity in Igfbp7+/+ and Igfbp7−/− primary hepatocytes. Both basal and LPS-induced luciferase activity was significantly increased in Igfbp7−/− hepatocytes when compared to Igfbp7+/+ (Fig. 4E). Igfbp7−/− hepatocytes and bone marrow-derived macrophages showed increased levels of phosphorylated p65 upon LPS treatment further confirming that Igfbp7 deletion results in activation of NF-κB (Fig. 4F and Fig. S7B).

We checked whether Igfbp7 status in the macrophages affects tumorigenesis by HCC cells. For this purpose we injected mouse HCC cells Dihxy (21) either alone or with Igfbp7+/+ or Igfbp7−/− bone marrow-derived macrophages at a tumor:macrophage ratio of 10:1 or 20:1 s.c. in NSG mice and monitored tumor development. Co-injection of Igfbp7−/− macrophages significantly stimulated tumorigenesis by Dihxy cells compared to Igfbp7+/+ cells indicating that Igfbp7 loss intrinsically changes macrophage properties rendering them more tumor-promoting (Fig. S7C). We cultured bone marrow-derived macrophages either in serum-free medium (control) or in conditioned media (CM) from Dihxy cells and analyzed expression of Il6 (marker for M1 macrophage) and Arg1 (marker for M2 macrophage) (Fig. S7D). Dihxy CM induced Il6 and Arg1 expression in both Igfbp7+/+ and Igfbp7−/− macrophages. However, this induction was more robust in Igfbp7−/− macrophages, especially for Arg1, indicating that Igfbp7−/− macrophages have a propensity for polarization to M2 subtype which promotes angiogenesis and tissue remodeling as well as immunosuppression (29–31).

RNA-sequencing (RNA-Seq) identifies inhibition of immune surveillance in Igfbp7−/− mice

To obtain insights into the gene expression changes facilitating HCC in Igfb7−/− mice we performed RNA-Seq using total RNA from naïve liver samples from 8 weeks old Igfbp7+/+ and −/− mice (n=3). Genes showing absolute fold-change of >1.5, FDR of <0.1 and p-value of <0.05 were selected. 473 genes showed differential changes, out of which 209 were upregulated and 264 were downregulated in Igfbp7−/− livers when compared to +/+ (Table S1). We performed biological processes and pathway analysis using the softwares DAVID and Ingenuity. Surprisingly, the topmost biological pathways identified to be inhibited in Igfbp7−/− livers are all associated with immune surveillance, such as antigen presentation or

dendritic cell (DC) maturation (Fig. 5A and Table S2). The genes regulating antigen presentation that are downregulated in Igfbp7−/− liver include MHC class I and II genes, proteasome components LMP2 and LMP7 that process the antigenic peptides, Transporter associated with Antigen Processing 1 (Tap1) that transports the processed peptide to the ER for assembly with MHC molecules, and co-stimulators CD80 and CD86. Downregulation of Tap1 mRNA in Igfbp7−/− liver was confirmed by Taqman Q-RT-PCR (Fig. 5B). Mature dendritic cells (DCs) present high cell surface expression of CD80 and CD86 (32). Downregulation of CD86 and CD80 in Igfbp7−/− $CD11b^{+}CD11c^{+}$ bone marrow-derived DCs (BMDCs) were confirmed by flow cytometry (Fig. 5C). Mean fluorescence intensity (MFI) for CD86 was 138 and 155, while MFI for CD80 was 240 and 165, respectively for Igfbp7+/+ and Igfbp7−/− DCs. Since there was a discrepancy between percentage of cell surface expression *versus* MFI for CD86 we confirmed these observations by biological assays. We measured antigen presentation capacity of BMDCs from 6 weeks old Igfbp7+/+ and −/− littermates. DCs, loaded with a tumor antigen gp100 peptide, was used to stimulate T cells from pmel-17 mice, a transgenic mouse expressing rearranged T cell receptor (TCR) recognizing gp100. T cell activation by Igfbp7−/− DCs was significantly blunted when compared to that by Igfbp7+/+ DCs as evidenced by decreased proliferation of T cells by $[^{3}H]$-thymidine incorporation assay and decreased production of IL-12 and IL-2 in the conditioned media (Fig. 5D). The inhibition in antigen presentation by Igfbp7−/− DCs could be rescued by addition of recombinant IGFBP7 protein (rIGFBP7) or treatment with OSI-906 (Fig. 5E). In Igfbp7−/− DCs, co-treatment of OSI-906 and rIGFBP7 did not further augment T-cell proliferation or IFN-γ production when compared to rIGFBP7 treatment alone although a significant increase in IL-2 production was observed. These findings suggest a possible IGF1R-independent function of IGFBP7. Treatment of Igfbp7+/+ DCs with rIGFBP7 did not modulate T-cell proliferation or IFN-γ or IL-2 production in antigen presentation assay suggesting a lack of activation of IGF signaling in these cells which may not be affected by rIGFBP7 or OSI-906 (Fig. S8A). Antigen presentation is positively regulated by IFN-γ that functions by stimulating the JAK-STAT1 pathway. Upon LPS treatment a substantial inhibition in STAT1 activation was observed in Igfbp7−/− DCs versus +/+ DCs indicating that IFN-γ signaling pathway is interfered in Igfbp7−/− DCs (Fig. 5F and S8B). To check potential role of Igfbp7 in regulating NK cell function splenocytes from Igfbp7+/+ and −/− mice were cultured in the presence of NK cell activating cytokines (IL-2 and IL-15) for 48 h and Granzyme B and IFN-γ production from NK cells (NK1.1+CD3-) was assayed by flow cytometry. No significant difference in NK cell activation was observed between Igfbp7+/+ and −/− indicating that Igfbp7 does not affect intrinsic functions of NK cells (Fig. S8C).

Overexpression of Igfbp7 decreases tumor growth by activating an anti-tumor immune response

As yet all studies analyzing the effect of IGFBP7, either recombinant protein, stable overexpression or via an adenovirus, have been performed in athymic nude mice thereby not detecting immunomodulatory properties of IGFBP7 (7). To examine the impact of IGFBP7 on tumor immune environment, we established stable pooled clone of mouse HCC Hepa1-6 cells overexpressing mIGFBP7 (BP7-OE). Overexpression of secreted mIGFBP7 in BP7-OE clones was confirmed by Western blot analysis in the conditioned media and by Q-RT-PCR

in the cells (Fig. 6A). Subcutaneous xenografts from BP7-OE cells grew significantly slower in syngeneic C57L mice, from which Hepa1-6 cells were established, compared to the control tumors (Fig. 6B). BP7-OE tumors showed decreased activation of Akt and ERK and marked decrease in CD31 staining confirming inhibition of IGF-1 signaling and angiogenesis (Fig. 6C and Fig. S9A–B). Interestingly, BP7-OE tumors presented with marked tumor infiltration of IFN-γ-producing $CD8^+$ or $CD4^+$ T cells (Fig. 6D), marked elevation of cytokine IL-12 (Fig. 6E), which is crucial for antitumor Th1 immunity, moderate elevation of IFN-γ (Fig. 6E) and decrease in MDSCs in the tumors (Fig. 6D). These tumors also showed significant upregulation of Tap1 (Fig. 6E). Collectively these findings in BP7-OE tumors reflect reverse findings of what is observed in Igfbp7−/− mice. To further confirm the role of induction of anti-tumor immunity, we established BP7-OE tumors in C57L mice and depleted $CD8^+$ and $CD4^+$ cells with neutralizing antibody. The depletion of $CD8^+$ or $CD4^+$ cells was confirmed by FACS analysis of the tumor (Fig. S9C). Depletion of $CD8^+$ and $CD4^+$ cells significantly rescued the growth of BP7-OE tumors, supporting a major role of immune activation in mediating tumor suppressor function of IGFBP7 (Fig. 6F).

Discussion

Previous studies in multiple tumor models, including HCC, have identified IGFBP7 as a potential tumor suppressor (7–9). However, an *in vivo* model is necessary to conclusively establish the tumor suppressor function of IGFBP7 and the present studies fulfil this need. We document that Igfbp7−/− mice develop spontaneous tumors in multiple organs, although not at 100% penetrance, and present with a pro-inflammatory *milieu* that might provide a fertile ground for sustenance and progression of cancers once cells become transformed following a mutagenic event. Indeed, hepatocarcinogenesis following DEN treatment is markedly accelerated in Igfbp7−/− mice compared to +/+ and +/− mice thereby establishing IGFBP7 as a *bona fide* tumor suppressor according to the two-hit hypothesis in which both alleles need to be mutated to manifest the tumorigenic phenotype.

The loss of Igfbp7 resulted in constitutive activation of IGF pathway in parenchymal cells, such as hepatocytes and MEFs, which translated into increased proliferation, accelerated cell cycle progression and inhibition of senescence. Activation of IGF-1 pathway protects from stress-induced premature senescence, IGFBP7 is induced in senescent cells and loss of IGFBP7 mediates escape from oncogene-induced senescence (8,33,34). In DEN-induced HCC model, DEN causes DNA damage, induces reactive oxygen species (ROS) and ultimately apoptosis in the hepatocytes (25). However, there is also compensatory proliferation to mitigate this effect. Upon activation of survival pathways, such as IGF-1, the damaged (and mutated) hepatocytes do not undergo apoptosis and continues to survive and proliferate resulting in expansion of mutated, transformed cells. Induction of senescence in pre-malignant cells and clearing of these senescent cells by immune system serves as a mechanism of inhibition of HCC (35). Thus deleting Igfbp7 in hepatocytes confers both proliferative and survival advantage and protection from senescence (Fig. 6G). On the other hand, we observed that the expression of IGFBP7 in macrophages is significantly more than that in hepatocytes suggesting an important role of IGFBP7 in modulating liver microenvironment. Igfbp7−/− macrophages show activation of NF-κB and increased

expression of pro-inflammatory cytokines thereby establishing a chronic inflammatory environment in which senescence-resistant transformed hepatocytes might thrive. Activated Akt, following activation of IGF-1R, phosphorylates IKK leading to activation of NF-κB pathway (36). Thus activation of IGF signaling might contribute to both proliferative and pro-inflammatory phenotypes (Fig. 6G).

Cross-talk between hepatocytes and macrophages is fundamental in HCC development. Macrophages require secreted factors, such as IL-1β, released from damaged hepatocytes, for activation, while damaged hepatocytes require macrophage-released factors, such as IL-6, for survival and proliferation and NF-κB plays an important role in regulating this cross-talk (26,37,38). The tumorigenic effects of NF-κB in HCC are highly dependent on cell type. For instance, hepatocytes specific knockout of IKKβ promoted DEN-induced HCC via increased ROS and hepatocyte compensatory proliferation, while double knockout of IKKβ in the macrophage and hepatocyte reduced DEN-induced HCC (25). In Igfbp7−/− mice NF-κB is activated in both hepatocytes and macrophages thereby creating a situation that is mirror image of IKKβ double knockout mice. The simultaneous activation of NF-κB in our model explains the concomitant increase in inflammatory cytokines, such as IL-6, IL1-β and TNFα, and the subsequent increase in Kupffer cell population in DEN-induced HCC.

One surprising finding deduced from our model is the ability of IGFBP7 to modulate the antigen presentation machinery and thereby an anti-tumor immune response. We document that deletion of Igfbp7 resulted in downregulation of an IFN-γ-regulated cluster of genes regulating antigen presentation. Indeed we observe decreased activation of IFN-γ signaling in Igfbp7−/− BMDCs which functionally translated into decreased antigen presentation and decreased infiltration of $CD8^+$ and $CD4^+$ T cells and NK cells in DEN-induced tumor. Treatment of Igfbp7−/− BMDCs with rIGFBP7 protein restored antigen presentation capacity in BMDCs documenting a key role of IGFBP7 in proper functioning of antigen presenting cells. As a corollary, overexpression of Igfbp7 in mouse HCC cells inhibited tumorigenesis in syngeneic mice with robust infiltration of $CD8^+$ and $CD4^+$ T cells and depletion of $CD8^+$ and $CD4^+$ T cells facilitated tumor growth. While the immunomodulatory effects of IGF-1 are less understood, several lines of evidence supports the potential involvement of IGF signaling in regulating tumor immunogenicity and immune cell phenotype or function. Silencing IGF-1 expression in Hepa1-6 cells increased its immunogenicity and decreased tumorigenicity by upregulation of MHC class I molecules and mobilization of T cells (39). In T cells IGF-1 treatment results in decreased surface expression of IFN-γR2 and inhibits IFN-γ-STAT1 signaling (40). Additionally, dendritic cells (DCs), upon treatment with IGF-1, showed a defect in maturation following LPS stimulation, and produced immune suppressive cytokines such as IL-10 (41). Indeed we observe an increase in arginase-1 and MDSCs in DEN-induced HCC in Igfbp7−/− mice and a decrease in MDSCs in BP7-OE tumors. Thus Igfbp7 deletion creates an immunosuppressive environment preventing clearance of transformed hepatocytes by the immune system (Fig. 6G).

In summary, we document that IGFBP7 can not only inhibit cancer cells but also modulate tumor microenvironment and this dual effect might have lasting effect in inhibiting both

primary tumors and distant metastasis. Even though HCC has an immunosuppressive *milieu*, immune targeted therapies are beginning to demonstrate significant objective responses in clinical trials. Targeted delivery of rIGFBP7 protein might be an effective therapeutic for HCC and other cancers.

Supplementary Material

Refer to Web version on PubMed Central for supplementary material.

Acknowledgments

PBF holds the Thelma Newmeyer Corman Chair in Cancer Research and is a Samuel Waxman Cancer Research Foundation (SWCRF) Investigator. XYW is the Mary Anderson Harrison Distinguished Professor in Cancer Research in VCU MCC. DS is the Harrison Foundation Distinguished Professor in Cancer Research in VCU MCC.

Financial support

The present study was supported in part by National Cancer Institute Grant R21 CA183954, National Institute of Diabetes and Digestive and Kidney Diseases Grant R01 DK107451 and VCU Massey Cancer Center (MCC) Pilot Project Grant (D. Sarkar), and R01 CA175033 and R01 CA154708 (X-Y. Wang). C.L. Robertson is supported by a National Institute of Diabetes And Digestive And Kidney Diseases Grant T32DK007150. Services in support of this project were provided by the VCU Massey Cancer Center Transgenic/Knock-out Mouse Facility and Flow Cytometry Facility, supported in part with funding from NIH-NCI Cancer Center Support Grant P30 CA016059.

Abbreviations

IGFBP7	Insulin-like growth factor binding protein-7
HCC	Hepatocellular carcinoma
MHC	Major histocompatibility complex
PI3K	Phosphatidylinositol-3-Kinase
ERK	Extracellular Signal-Regulated Kinase
GSK3β	Glycogen synthase kinase 3β
PCNA	Proliferating cell nuclear antigen
AFP	α-feto protein
MTT	3-(4,5-Dimethylthiazol-2-Yl)-2,5-Diphenyltetrazolium Bromide
BrdU	5-bromo-2′-deoxyuridine
MDSC	Myeloid-derived suppressor cells
BMDC	Bone marrow-derived dendritic cells
NK	Natural killer cells
NSG	NOD *scid* Gamma
CM	Conditioned media

References

1. Swann JB, Smyth MJ. Immune surveillance of tumors. J Clin Invest. 2007; 117:1137–46. [PubMed: 17476343]
2. Mittal D, Gubin MM, Schreiber RD, Smyth MJ. New insights into cancer immunoediting and its three component phases--elimination, equilibrium and escape. Curr Opin immunol. 2014; 27:16–25. [PubMed: 24531241]
3. Neefjes J, Jongsma ML, Paul P, Bakke O. Towards a systems understanding of MHC class I and MHC class II antigen presentation. Nat Rev Immunol. 2011; 11:823–36. [PubMed: 22076556]
4. Makarova-Rusher OV, Medina-Echeverz J, Duffy AG, Greten TF. The yin and yang of evasion and immune activation in HCC. J Hepatol. 2015; 62:1420–9. [PubMed: 25733155]
5. Scharf JG, Braulke T. The role of the IGF axis in hepatocarcinogenesis. Hormone Metab Res. 2003; 35:685–93.
6. Evdokimova V, Tognon CE, Benatar T, Yang W, Krutikov K, Pollak M, et al. IGFBP7 binds to the IGF-1 receptor and blocks its activation by insulin-like growth factors. Sci Signal. 2012; 5:ra92. [PubMed: 23250396]
7. Chen D, Yoo BK, Santhekadur PK, Gredler R, Bhutia SK, Das SK, et al. Insulin-like growth factor-binding protein-7 functions as a potential tumor suppressor in hepatocellular carcinoma. Clin Cancer Res. 2011; 17:6693–701. [PubMed: 21908579]
8. Wajapeyee N, Serra RW, Zhu X, Mahalingam M, Green MR. Oncogenic BRAF induces senescence and apoptosis through pathways mediated by the secreted protein IGFBP7. Cell. 2008; 132:363–74. [PubMed: 18267069]
9. Sprenger CC, Damon SE, Hwa V, Rosenfeld RG, Plymate SR. Insulin-like growth factor binding protein-related protein 1 (IGFBP-rP1) is a potential tumor suppressor protein for prostate cancer. Cancer Res. 1999; 59:2370–5. [PubMed: 10344746]
10. Li F, Fan YC, Gao S, Sun FK, Yang Y, Wang K. Methylation of serum insulin-like growth factor-binding protein 7 promoter in hepatitis B virus-associated hepatocellular carcinoma. Genes Chromosomes Cancer. 2014; 53:90–7. [PubMed: 24142767]
11. Wajapeyee N, Kapoor V, Mahalingam M, Green MR. Efficacy of IGFBP7 for treatment of metastatic melanoma and other cancers in mouse models and human cell lines. Mol Cancer Ther. 2009; 8:3009–14. [PubMed: 19861408]
12. Chen D, Siddiq A, Emdad L, Rajasekaran D, Gredler R, Shen XN, et al. Insulin-like growth factor-binding protein-7 (IGFBP7): a promising gene therapeutic for hepatocellular carcinoma (HCC). Mol Ther. 2013; 21:758–66. [PubMed: 23319057]
13. Bissell DM, Guzelian PS. Degradation of endogenous hepatic heme by pathways not yielding carbon monoxide. Studies in normal rat liver and in primary hepatocyte culture. J Clin Invest. 1980; 65:1135–40. [PubMed: 7364941]
14. Bissell DM, Guzelian PS. Degradation of endogenous hepatic heme by pathways not yielding carbon monoxide. Studies in normal rat liver and in primary hepatocyte culture. J Clin Invest. 1980; 65:1135–40. [PubMed: 7364941]
15. Xu J. Preparation, culture, and immortalization of mouse embryonic fibroblasts. Current Protoc Mol Biol. 2005 Chapter 28:Unit 28 1.
16. Zhang X, Goncalves R, Mosser DM. The isolation and characterization of murine macrophages. Current Protoc Immunol. 2008 Chapter 14:Unit 14 1.
17. Maschmeyer P, Flach M, Winau F. Seven steps to stellate cells. J Vis Exp. 2011; 51:2710.
18. Guo C, Yi H, Yu X, Hu F, Zuo D, Subjeck JR, et al. Absence of scavenger receptor A promotes dendritic cell-mediated cross-presentation of cell-associated antigen and antitumor immune response. Immunol Cell Biol. 2012; 90:101–8. [PubMed: 21383767]
19. Yu X, Guo C, Yi H, Qian J, Fisher PB, Subjeck JR, et al. A multifunctional chimeric chaperone serves as a novel immune modulator inducing therapeutic antitumor immunity. Cancer Res. 2013; 73:2093–103. [PubMed: 23333935]
20. Robertson CL, Srivastava J, Siddiq A, Gredler R, Emdad L, Rajasekaran D, et al. Genetic deletion of AEG-1 prevents hepatocarcinogenesis. Cancer Res. 2014; 74:6184–93. [PubMed: 25193383]

21. He G, Dhar D, Nakagawa H, Font-Burgada J, Ogata H, Jiang Y, et al. Identification of liver cancer progenitors whose malignant progression depends on autocrine IL-6 signaling. Cell. 2013; 155:384–96. [PubMed: 24120137]
22. Lee JS, Chu IS, Mikaelyan A, Calvisi DF, Heo J, Reddy JK, et al. Application of comparative functional genomics to identify best-fit mouse models to study human cancer. Nat Genet. 2004; 36:1306–11. [PubMed: 15565109]
23. Lim IK. Spectrum of molecular changes during hepatocarcinogenesis induced by DEN and other chemicals in Fischer 344 male rats. Mech Ageing Dev. 2002; 123:1665–80. [PubMed: 12470904]
24. Sakurai T, He G, Matsuzawa A, Yu GY, Maeda S, Hardiman G, et al. Hepatocyte necrosis induced by oxidative stress and IL-1 alpha release mediate carcinogen-induced compensatory proliferation and liver tumorigenesis. Cancer Cell. 2008; 14:156–65. [PubMed: 18691550]
25. Maeda S, Kamata H, Luo JL, Leffert H, Karin M. IKKbeta couples hepatocyte death to cytokine-driven compensatory proliferation that promotes chemical hepatocarcinogenesis. Cell. 2005; 121:977–90. [PubMed: 15989949]
26. Pikarsky E, Porat RM, Stein I, Abramovitch R, Amit S, Kasem S, et al. NF-kappaB functions as a tumour promoter in inflammation-associated cancer. Nature. 2004; 431:461–6. [PubMed: 15329734]
27. Fletcher M, Ramirez ME, Sierra RA, Raber P, Thevenot P, Al-Khami AA, et al. l-Arginine depletion blunts antitumor T-cell responses by inducing myeloid-derived suppressor cells. Cancer Res. 2015; 75:275–83. [PubMed: 25406192]
28. Ben-Neriah Y, Karin M. Inflammation meets cancer, with NF-kappaB as the matchmaker. Nat Immunol. 2011; 12:715–23. [PubMed: 21772280]
29. Qian BZ, Pollard JW. Macrophage diversity enhances tumor progression and metastasis. Cell. 2010; 141:39–51. [PubMed: 20371344]
30. Mantovani A, Allavena P, Sica A. Tumour-associated macrophages as a prototypic type II polarised phagocyte population: role in tumour progression. Eur J Cancer. 2004; 40:1660–7. [PubMed: 15251154]
31. Lewis CE, Pollard JW. Distinct role of macrophages in different tumor microenvironments. Cancer Res. 2006; 66:605–12. [PubMed: 16423985]
32. Banchereau J, Briere F, Caux C, Davoust J, Lebecque S, Liu YJ, et al. Immunobiology of dendritic cells. Ann Rev Immunol. 2000; 18:767–811. [PubMed: 10837075]
33. Gruber HE, Hoelscher GL, Ingram JA, Bethea S, Hanley EN. IGF-1 rescues human intervertebral annulus cells from in vitro stress-induced premature senescence. Growth Factors. 2008; 26:220–5. [PubMed: 19021034]
34. Swisshelm K, Ryan K, Tsuchiya K, Sager R. Enhanced expression of an insulin growth factor-like binding protein (mac25) in senescent human mammary epithelial cells and induced expression with retinoic acid. Proc Natl Acad Sci USA. 1995; 92:4472–6. [PubMed: 7538673]
35. Kang TW, Yevsa T, Woller N, Hoenicke L, Wuestefeld T, Dauch D, et al. Senescence surveillance of pre-malignant hepatocytes limits liver cancer development. Nature. 2011; 479:547–51. [PubMed: 22080947]
36. Mitsiades CS, Mitsiades N, Poulaki V, Schlossman R, Akiyama M, Chauhan D, et al. Activation of NF-kappaB and upregulation of intracellular anti-apoptotic proteins via the IGF-1/Akt signaling in human multiple myeloma cells: therapeutic implications. Oncogene. 2002; 21:5673–83. [PubMed: 12173037]
37. Karin M, Cao Y, Greten FR, Li ZW. NF-kappaB in cancer: from innocent bystander to major culprit. Nat Rev Cancer. 2002; 2:301–10. [PubMed: 12001991]
38. Finkin S, Yuan D, Stein I, Taniguchi K, Weber A, Unger K, et al. Ectopic lymphoid structures function as microniches for tumor progenitor cells in hepatocellular carcinoma. Nat Immunol. 2015; 16:1235–44. [PubMed: 26502405]
39. Liu Y, Wang H, Zhao J, Ma J, Wei L, Wu S, et al. Enhancement of immunogenicity of tumor cells by cotransfection with genes encoding antisense insulin-like growth factor-1 and B7.1 molecules. Cancer Gene Ther. 2000; 7:456–65. [PubMed: 10766352]

40. Bernabei P, Bosticardo M, Losana G, Regis G, Di Paola F, De Angelis S, et al. IGF-1 down-regulates IFN-gamma R2 chain surface expression and desensitizes IFN-gamma/STAT-1 signaling in human T lymphocytes. Blood. 2003; 102:2933–9. [PubMed: 12842994]

41. Huang CT, Chang MC, Chen YL, Chen TC, Chen CA, Cheng WF. Insulin-like growth factors inhibit dendritic cell-mediated anti-tumor immunity through regulating ERK1/2 phosphorylation and p38 dephosphorylation. Cancer Lett. 2015; 359:117–26. [PubMed: 25592043]

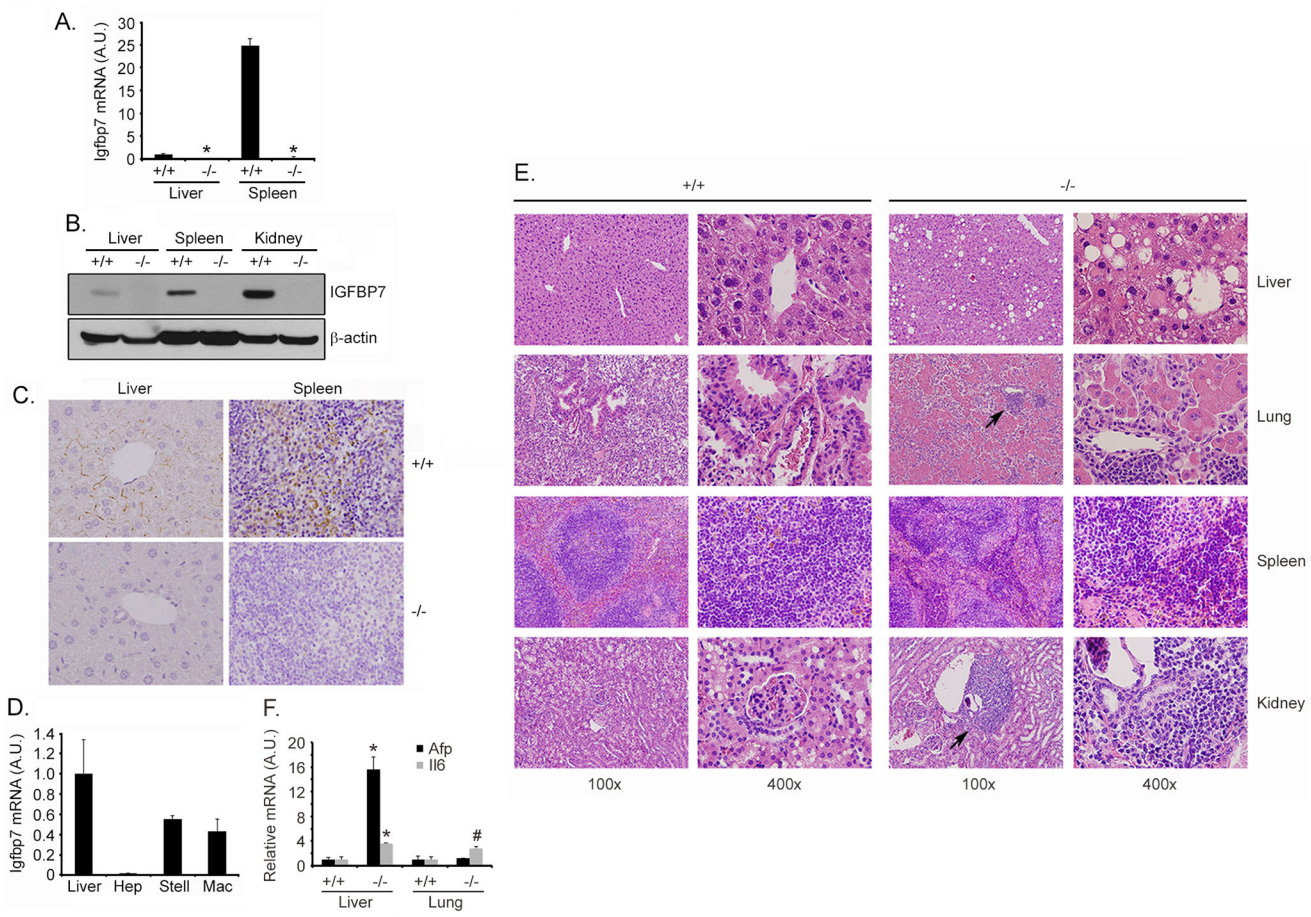

Figure 1.

Igfbp7−/− mice develop spontaneous tumors. A. Igfbp7 mRNA levels in livers and spleens of Igfbp7+/+ and Igfbp7−/− mice. B. IGFBP7 protein levels in the indicated organs. β-actin: loading control. C. Immunohistochemistry for IGFBP7 in sections of liver and spleen of adult mice. D. Igfbp7 mRNA levels in total liver and in hepatocytes (Hep), stellate cells (Stell) and peritoneal macrophages (Mac). E. H&E staining of sections of the indicated organs in 24 months old mice. Arrows indicate lymphocytic infiltration. F. Afp and Il6 mRNA levels in livers and lungs of 24 months old Igfbp7+/+ and Igfbp7−/− mice. For graphs, data represent mean ± SD. *: $p<0.01$; #: $p<0.05$. A.U.: arbitrary unit. For all analyses at least 3 mice or more were used per group.

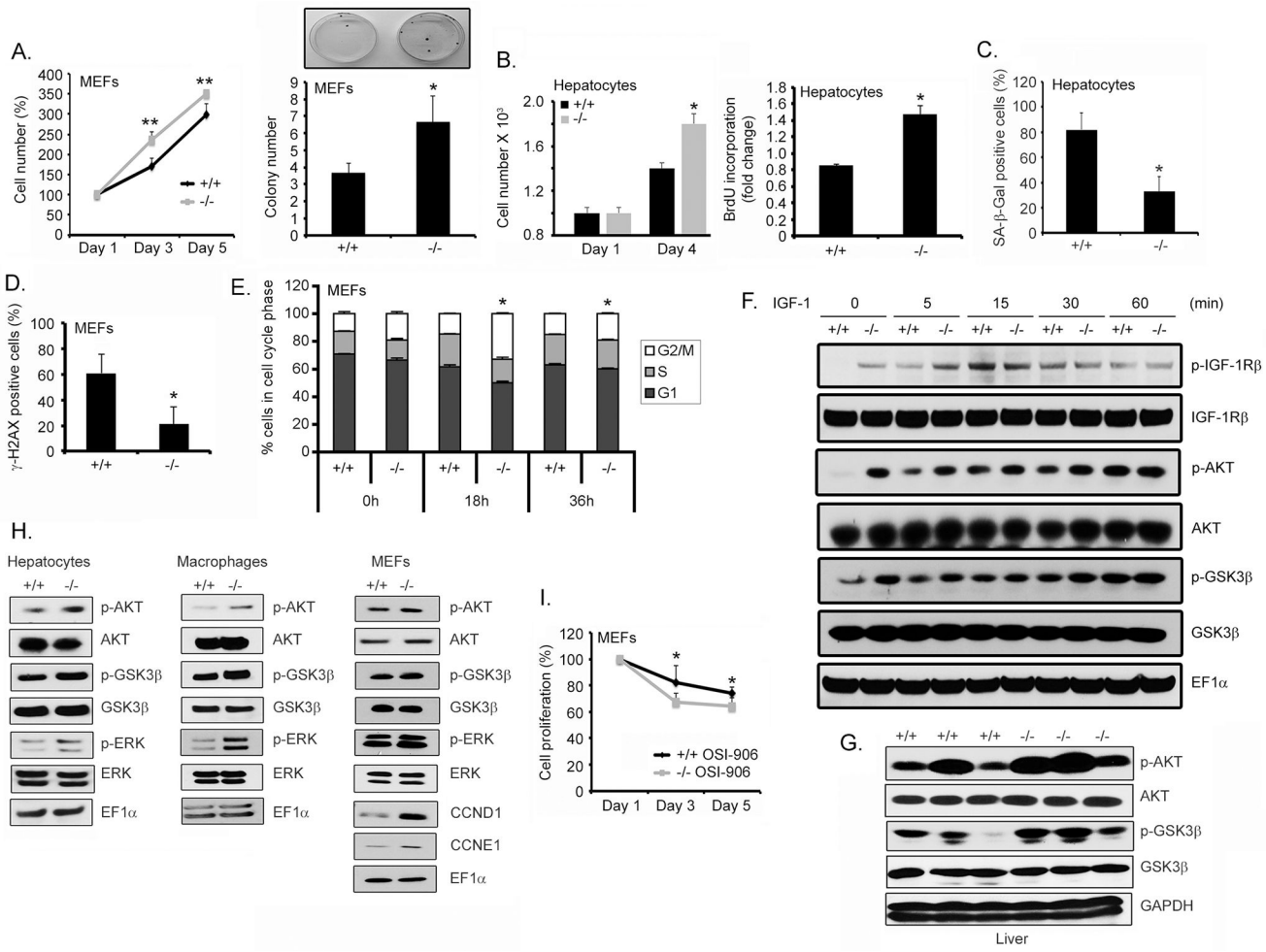

Figure 2.

Loss of Igfbp7 increases proliferation and inhibits senescence by activating IGF signaling pathway. A. Cell proliferation (left) and colony formation assays (right) in mouse embryonic fibroblasts (MEFs). B. Cell proliferation (left) and IGF-1-stimulated BrdU incorporation assays (right) in hepatocytes. C. Senescence-associated β-galactosidase (SA-β-Gal)-positive hepatocytes at day 8 of culture. D. γ-H2AX positive MEFs after 12 h of serum starvation. E. Cell cycle analysis of MEFs at 18 and 36 h after release from serum-free medium. F. Hepatocytes were cultured in insulin-free medium for 12 hours prior to treatment with IGF-1 (20ng/mL) for the indicated time points. Western blot analyses for the indicated proteins were performed. G. Western blot analysis for the indicated proteins in liver lysates of three independent Igfbp7+/+ and Igfbp7−/− mice. H. Western blot analysis for the indicated proteins in the indicated cells isolated from adult mice. For each cell type a representative EF1α blot is shown as loading control. I. Cell proliferation analysis in MEFs upon treatment with OSI-906 (4 μmol/L). For graphs, data represent mean ± SD. *: $p<0.01$.

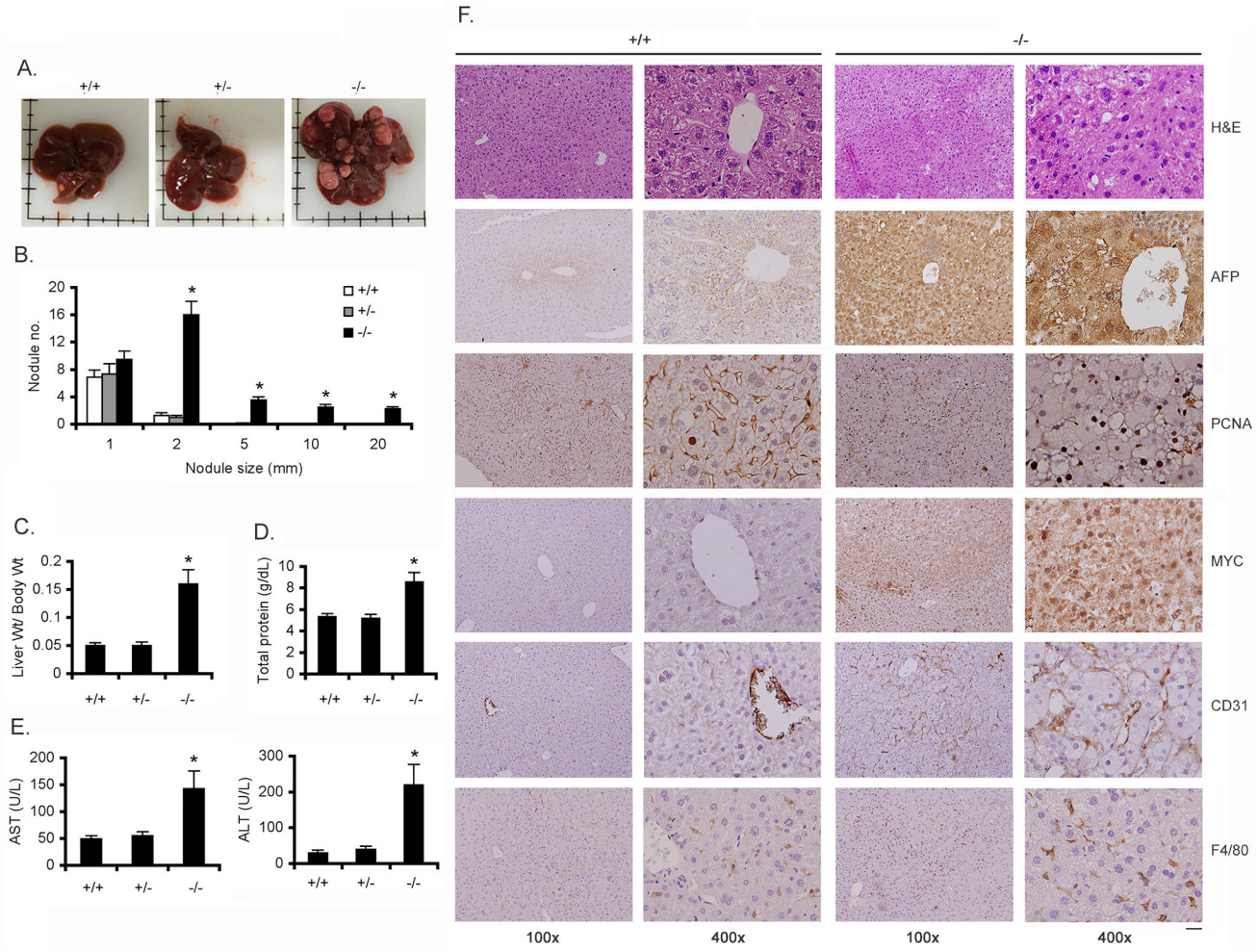

Figure 3.

Genetic deletion of Igfbp7 accelerates DEN-induced HCC. Mice were treated with DEN (10 μg/gm) at 2 wks of age and were sacrificed at 32 wks. A. Photograph of DEN-treated mouse livers of the indicated genotypes. B. Number and sizes of liver nodules. C. Liver weight of DEN-injected mice. D–E. Total protein (D) and Aspartate aminotransferase (AST) and Alanine aminotransferase (ALT) (E) levels in DEN-injected mouse sera. For B–E, n = 15 mice for +/+, 12 mice for +/− and 11 mice for −/−. F. H&E and immunostaining for the indicated proteins in liver sections. Scale bar: 20 μm. For graphs, data represent mean ± SD. *: $p<0.01$.

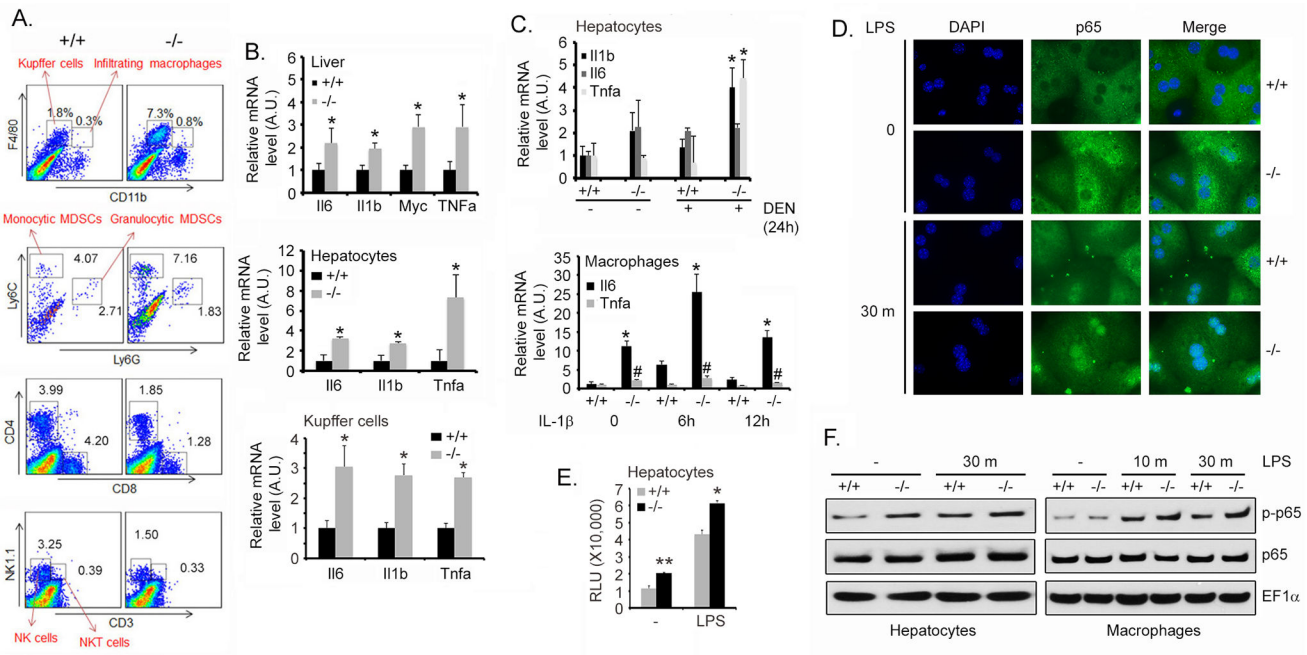

Figure 4.

Loss of Igfbp7 generates an inflammatory and immunosuppressive environment. A. Immune profile of DEN-treated Igfbp7+/+ and Igfbp7−/− mice at 20 weeks. B. Levels of the indicated mRNAs in the livers of DEN-injected mice at 32 wks (top), in hepatocytes isolated from DEN-injected mice at 24 wks (middle), and in Kupffer cells isolated from DEN-injected mice at 5 wks (bottom). C. Levels of the indicated mRNAs in hepatocytes *in vitro* treated with DEN for 24 h (top). Levels of the indicated mRNAs in macrophages treated or not with IL-1β (10 ng/ml) for 6 or 12h. D. Immunofluorescence for p65 NF-κB in hepatocytes treated with LPS (500 ng/mL) for 30 min. E. NF-κB luciferase reporter activity was measured in Igfbp7+/+ and Igfbp7−/− hepatocytes. Firefly luciferase activity was normalized by Renilla luciferase activity. The activity of empty pGL3-basic vector was considered as 1. R.L.U.: Relative luciferase units. F. Western blot analysis for the indicated proteins in LPS-treated hepatocytes and bone marrow-derived macrophages. For graphs, data represent mean ± SD. *: $p<0.01$; **: $p<0.05$; #: $p<0.04$. For all analyses at least 3 mice or more were used per group. A.U.: arbitrary unit.

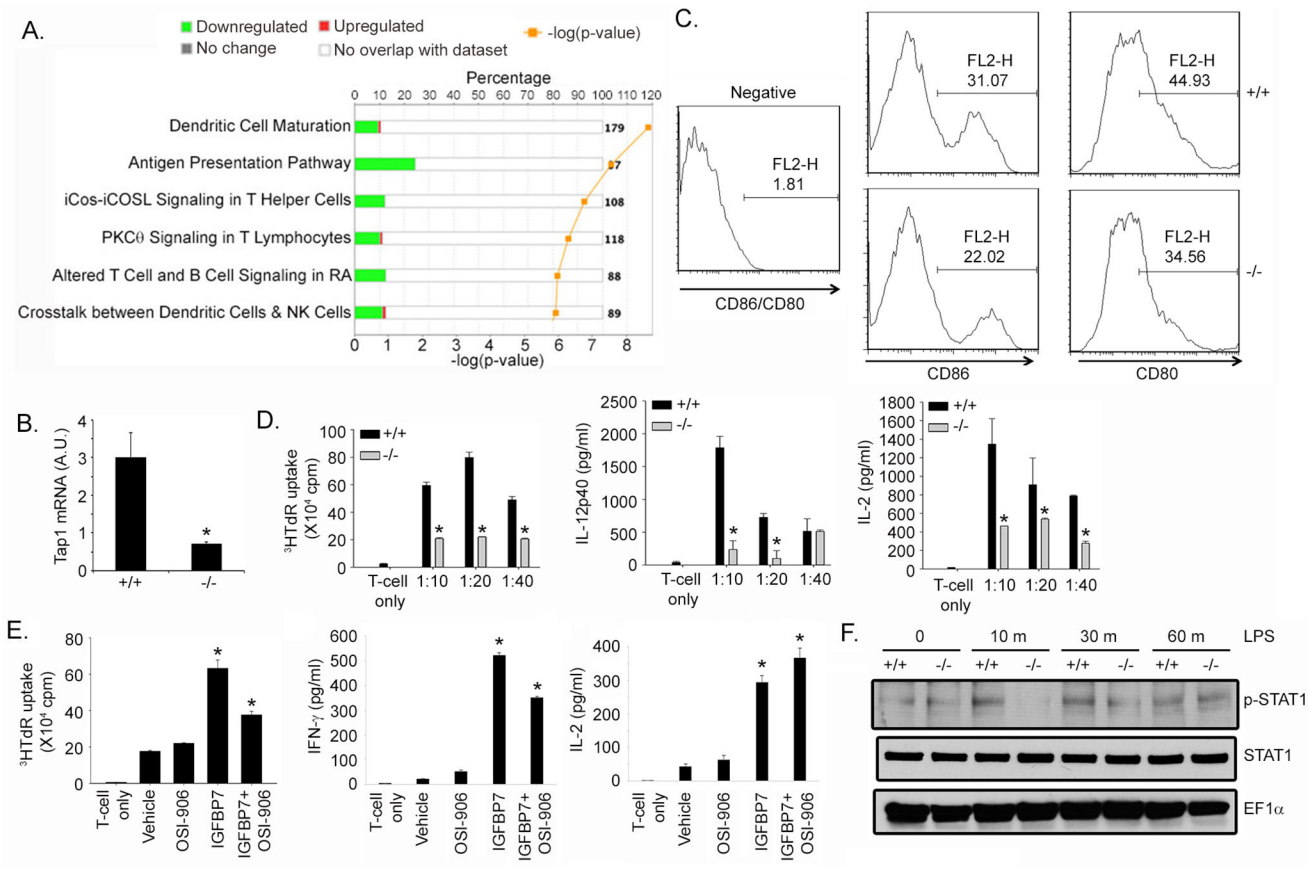

Figure 5.

Inhibition of immunosurveillance in Igfbp7−/− mice. A. Top biological pathways downregulated in naive Igfbp7−/− livers. B. Tap1 mRNA levels in total liver. C. Levels of CD86 and CD80 in bone marrow-derived dendritic cells (BMDCs). D. Donor pmel-17 T cells were co-cultured with BMDCs pulsed with gp100 at the indicated molar ratios (DC:TC) for 60 h with 2 h pre-treatment with LPS (500 ng/mL) for priming. ^{3}H-thymidine (^{3}HTdR) incorporation was measured (left). IL-12p40 (middle) and IL-2 (right) levels were measured in the media by ELISA. E. gp100-loaded Igfbp7−/− BMDCs were treated or not with rIGFBP7 protein for 3 h followed by OSI-906 (4 μmol/L) for 2 h and LPS (500 ng/mL) for 2 h. The cells were washed and co-cultured with pmel-17 T cells for 60 h. ^{3}H-thymidine (^{3}HTdR) incorporation was measured (left). IFN-γ (middle) and IL-2 (right) levels were measured in the media by ELISA. F. BMDCs were treated with LPS (500 ng/mL) for the indicated time points and Western blot analysis was performed for the indicated proteins. For graphs, data represent mean ± SD. *: $p<0.01$.

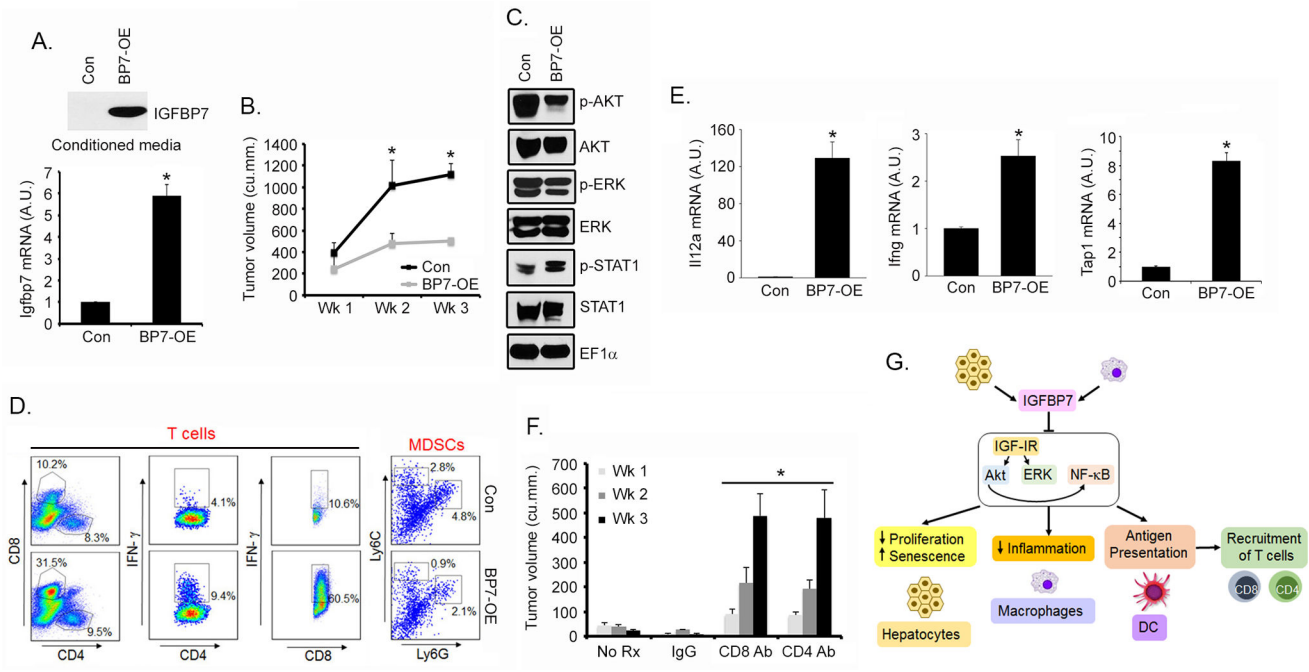

Figure 6.

Overexpression of Igfbp7 decreases tumor growth and stimulates an anti-tumor immune response. A. IGFBP7 protein levels in the conditioned media (top) and Igfbp7 mRNA levels in the cells (bottom) of control and IGFBP7-overexpressing clone (BP7-OE) of Hepa1-6 cells. B. The indicated clones ($1X10^6$ cells) were injected s.c. in C57L mice (n=5 per group) and tumor volume was measured. C. Levels of the indicated proteins in tumor lysates at the end of the study. D. IFN-γ-producing $CD8^+$ or $CD4^+$ T cells and MDSCs in the tumors at the end of the study. E. Il12a (left), Ifng (middle) and Tap1 (right) mRNA levels in the tumors at the end of the study. F. BP7-OE cells were injected s.c. in C57L mice (n=5 per group) and treated with Control IgG and $CD8^+$ or $CD4^+$ neutralizing antibodies (200 μg i.p.). Tumor volume was measured. For all graphs, the data represent mean ± SD; *: $p<0.01$. G. Schematic representation of the molecular mechanism by which IGFBP7 suppresses tumors. IGFBP7, secreted from hepatocytes, inhibits IGF and NF-κB signaling in macrophages preventing inflammation. IGFBP7, secreted from the microenvironment cells, inhibits IGF and NF-κB signaling in hepatocytes thus impeding proliferation and inducing senescence. IGFBP7 promotes antigen presentation by dendritic cells resulting in recruitment of CD4+ and CD8+ cells. These effects collectively protect from HCC. In addition to the paracrine effects depicted in this diagram there might be autocrine effects regulating the same end-points.